RB6 Nanowires

Subjects: Nanoscience & Nanotechnology
Contributor: Wei Han

With the rise of topological insulator samarium hexaboride (SmB6), rare-earth hexaboride (RB6) nanowires are the focus of the second wave of a research boom. Recent research has focused on new preparation methods, novel electronic properties, and extensive applications.

nanowire field emission chemical vapor deposition

1. Introduction

Rare-earth hexaborides (RB_6) have received substantial attention thanks to their high electrical conductivity, high melting points, and high chemical stability. Meanwhile, the strong correlation effect of 4f–5d electrons of rare-earth elements also brings some newfangled physical properties of RB_6 [1][2][3]. For example, yttrium hexaboride (YB_6) is a superconductor with a Tc of 7.2 K, which is the second highest transition temperature among all borides [4]. Moreover, lanthanum hexaboride (LaB_6), possessing low work function of 2.7 eV, is a famous thermionic electron emission material with high current density and stability [5]. Cerium hexaboride (CeB_6) is an antiferromagnetic heavy-fermion metal, but recently, it was found to demonstrate low-energy ferromagnetic fluctuation [6]. Furthermore, as a ferromagnetic semimetal, europium hexaboride (EuB_6) recently exhibited a colossal magnetoresistance effect [7]. In recent years, the emergent topological insulator has increased interest in samarium hexaboride (SmB_6), which possesses both insulating bulk state and metallic surface state due to the inversion of the d and f bands. Experimental evidence proves that SmB_6 is the first strongly correlated 3D topological Kondo insulator [8].

Due to the small size effect and quantum confinement effect, one-dimensional (1D) nanomaterials have new properties compared with bulk crystals. With the rise of 1D nanomaterials, RB_6 experienced the first wave of a research boom from 2005 to 2015, and many RB_6 nanowires were prepared by chemical vapor deposition (CVD) [9][10][11][12][13][14][15][16][17][18][19][20]. These RB_6 nanowires achieved excellent field emission properties and mechanical properties [21][22][23][24][25][26][27][28][29]. From 2016, the second wave of research boom of RB_6 began as SmB_6 proved to be a topological insulator, and researchers began to explore the difference in topological properties between nanowires and bulk single crystals [8].

2. Properties and Applications of RB_6 Nanowires

2.1. Electronic Transportation

As an emerging topological insulator, many experiments and theoretical studies have been conducted on bulk SmB_6 single crystals [8]. From 2016, researchers began to investigate the novel electronic transport and magneto-transport properties of SmB_6 nanowires [30][31][32][33][34][35][36][37]. In 2017, Kong et al. reported the spin-polarized surface state transport of single SmB_6 nanowires (**Figure 1**a–c) [33]. Under 5 K, the resistance appears saturated and flat, indicating that the surface states control the transport behavior. The appearance of topological surface states is caused by the reversal of *d* and *f* electrons. The fitting of a temperature-dependent resistance curve reveals that SmB_6 nanowire has a bulk gap ~3.2 meV, which is opened by the hybridization of the 4*f* bands and 5*d* bands in SmB_6 nanowires. As shown in **Figure 1**c, the magnetoresistance (MR) of SmB_6 nanowires is negative and the MR shows no sign of saturation at high magnetic field up to 14 T. The negative MR indicates that this transport behavior is spin-dependent. Furthermore, the nonlocal tests reveal that the surface state transport of SmB_6 nanowires is spin-polarized. In another interesting work, Zhou et al. reported the positive planar Hall effect (PHE) of SmB_6 nanowires (**Figure 1**d–f) [34]. They found that as the temperature decreases, the amplitude increases sharply, but saturates at 5 K. This positive PHE is due to the surface states of SmB_6. In other studies, the researchers found the anomalous magnetoresistance and the hysteresis of magnetoresistance in SmB_6 nanowires [35][36][37].

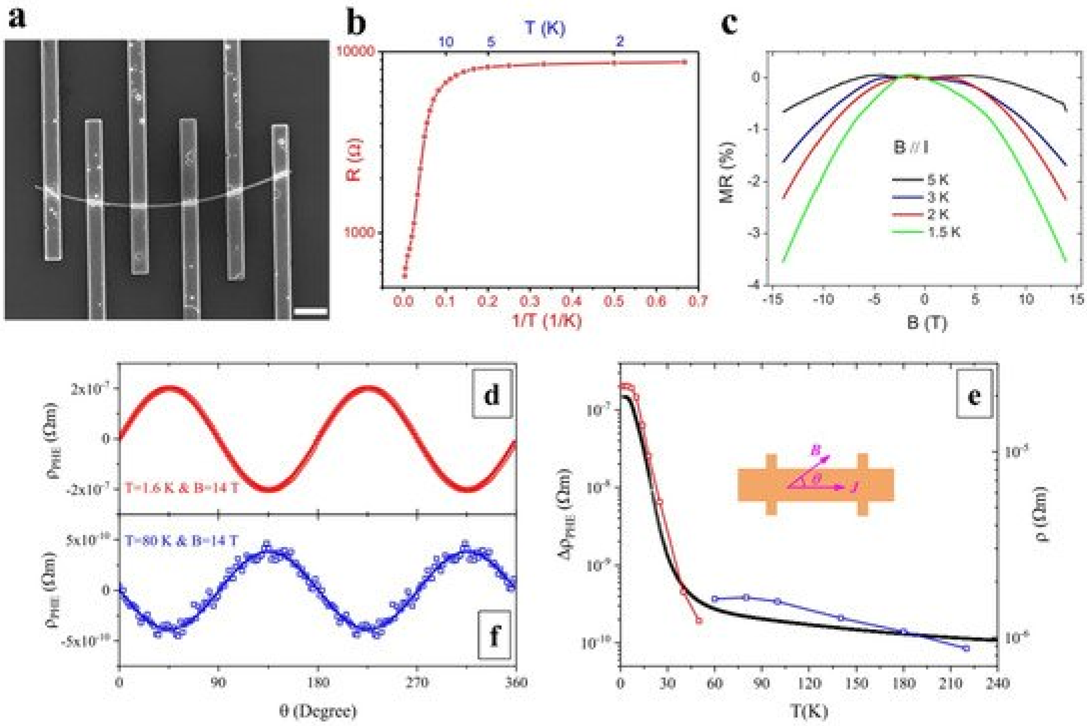

Figure 1. (**a**) SEM image of a SmB_6 nanowire device, the scalebar is 2 μm. (**b**) Temperature-dependent resistance of the SmB_6 nanowire. (**c**) Magnetoresistance curves under a parallel magnetic field at various temperatures [33]. Copyright 2017, American Physical Society. (**d**) Planar Hall resistivity with various angles at 1.6 K. (**e**) PHE amplitude and resistivity. Inset is the definition of tilting angle θ. (**f**) Planar Hall resistivity with various angles at 80 K [34]. Copyright 2019, American Physical Society.

In the RB_6 family, like SmB_6, YbB_6 is proposed to be a mixed-valent (Yb^{2+}/Yb^{3+}) topological insulator and demonstrates new quantum phenomena [38][39][40]. In 2018, Han et al. reported the semiconductor–insulator transition behavior in a YbB_6 nanowire (**Figure 2**) [41]. As shown in **Figure 2**b, as the temperature decreases from 300 to 2 K, the resistivity of the YbB_6 nanowire device undergoes a dramatic 49-fold increase ($\rho_{2\ K}/\rho_{300\ K} = 49$). They propose that the semiconductor–insulator transition is due to a small band gap opening at a low temperature induced by the slightly boron-rich or boron-deficient segments in YbB_6 nanowires. Furthermore, the magnetoresistance (MR) of the YbB_6 nanowire was tested with perpendicular magnetic field B = 0–7 T at various temperatures. As displayed in **Figure 2**c, the MR shows no sign of saturation at high magnetic field up to 14 T and has a linear dependence with B^2 at 2 K and 10 K, which follows Kohler's law. Because a semiconductor–insulator transition occurred at 2 K for YbB_6 nanowires, the hole-dominant transport is credible at 2 K and the transport at 10 K is electron-dominant.

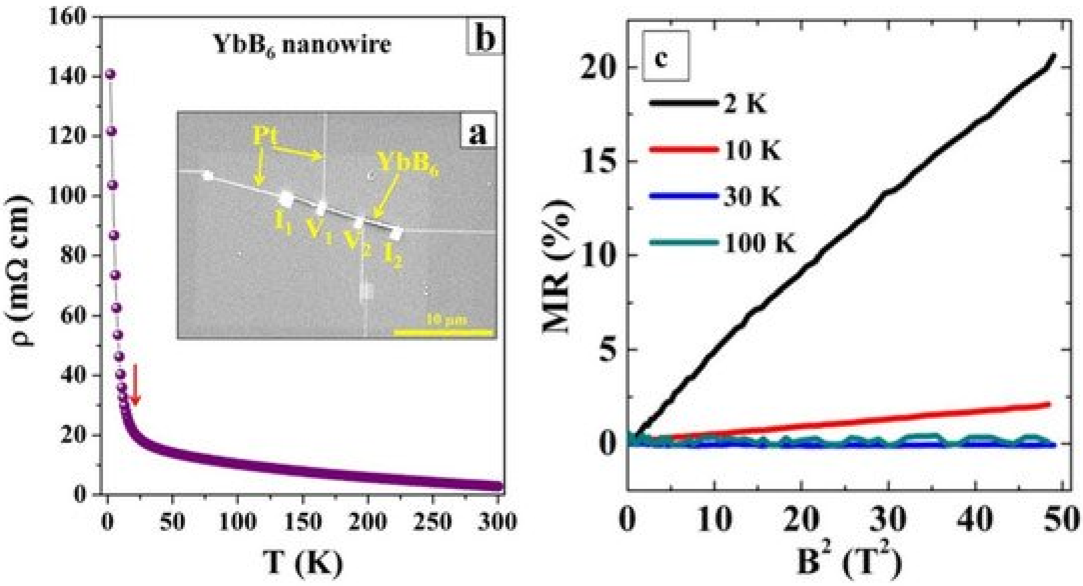

Figure 2. (**a**) SEM image of the YbB_6 nanowire device. (**b**) Resistivity as a function of temperature from 2 to 300 K. (**c**) Magnetoresistance (MR) as a function of B^2 at various temperatures [41]. Copyright 2018, Elsevier Science B.V.

Of all the metal borides, YB_6 bulk crystals have the second highest superconducting transition temperature of 7.2 K after MgB_2. More superconducting properties have been studied in bulk YB_6 single crystals, but the superconducting properties of YB_6 nanowires have not been reported. Recently, Wang et al. reported the synthesis of 1D YB_6 nanowires by a high-pressure solid-state method and studied their magnetic properties (**Figure 3**). The temperature-dependent magnetization under zero-field cooling and field cooling revealed that the YB_6 nanowires have a superconducting transition with T_c = 7.8 K. Meanwhile, they found that the YB_6 nanowires exhibited a peak effect in the superconducting state observed from the magnetic hysteresis loops obtained at 2 K and 10 K, indicating that YB_6 nanowires pertain to a type-II superconductor.

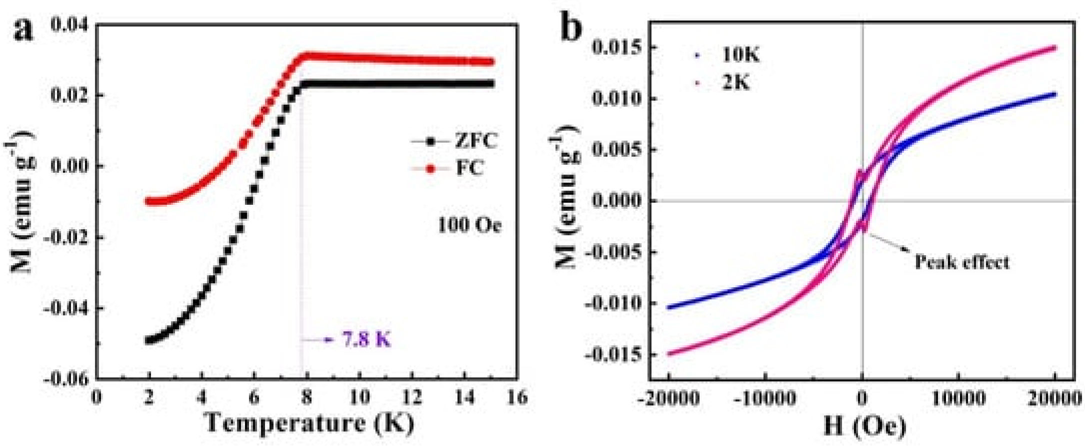

Figure 3. (**a**) The temperature-dependent magnetization under zero-field cooling and field cooling modes of superconducting YB_6 nanostructure. (**b**) The magnetic hysteresis loops obtained at 2 K and 10 K [42]. Copyright 2021, Elsevier Science B.V.

LaB_6 bulk single crystals have been applied in commercial scanning electron microscopy and transmission electron microscopy. For RB_6 nanowires, the most attractive application is also the field emitter of an electronic gun of an electron microscope (**Figure 4**) [43][44][45]. Published in Nature Nanotechnology, Zhang et al. reported the first application of a single LaB_6 nanowire to scanning electron microscopy, revealing excellent performance [43]. Their LaB_6 nanowire electron source shows low work function, is chemically inert, and has high monochromaticity. When assembled into a field-emission gun of SEM, it demonstrates ultra-low emission decay, and its current density gain is three orders of magnitude higher than traditional W tips. By this LaB_6 nanowire-based SEM, they obtained low-noise and high-resolution images, better than W-tip-based SEM. Recently, published in Nature Nanotechnology in 2021, Zhang et al. reported the installation of a single LaB_6 nanowire into an aberration-corrected transmission electron microscope [44]. The LaB_6 NW-based TEM achieved atomic resolution and probe-forming modes at 60 kV energy. Compared with the state-of-the-art W (310) electron source, the nanostructured electron source provides higher temporal coherence at a spatial frequency of 105 pm, showing a higher contrast transfer amplitude of 84% and a spectral energy resolution of 35%. The first demonstration of the LaB_6 nanowire electron source in SEM and TEM reveals that the RB_6 nanowires have notable application prospects and commercial value both in electron microscopy and other electron-emitting devices.

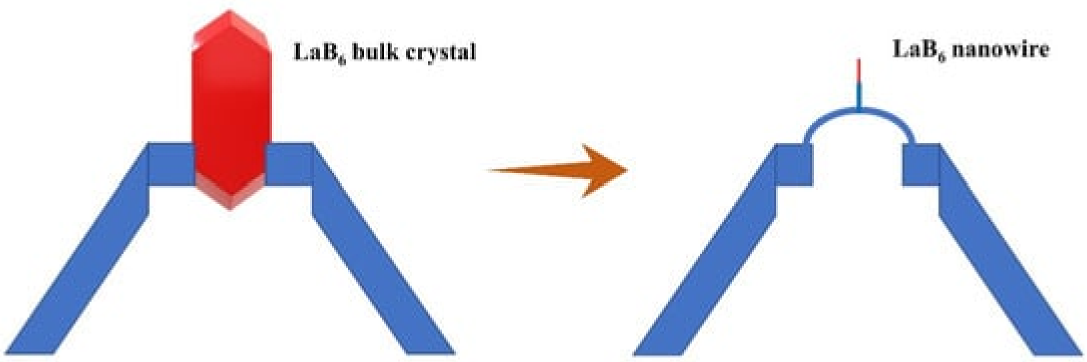

Figure 4. Illustrations of the LaB_6 bulk crystal and nanowire electron-emission sources in electron microscopy.

2.2. Optoelectronic Properties

Most of the RB_6 crystals are metals with zero band gap, and thus, they are not suitable for semiconductor devices, such as field effect transistors and photodetectors. However, as a topological Kondo insulator, SmB_6 shows a small gap (3 meV), evidenced by electrical transport measurements, and may have potential in fabricating devices. Recently, Zhou et al. [46] first reported the self-powered SmB_6 nanowire photodetectors with broadband wavelengths covering from 488 nm to 10.6 μm (**Figure 5**). They claimed that the photocurrent stemmed from the interface of SmB_6 nanowire and Au electrodes owing to the built-in potential, proved by the spatially resolved photocurrent mapping. The current on/off ratio, responsibility, and specific detectivity are 100, 1.99 mA/W, and 2.5 × 10^7 Jones, respectively. The demonstration of a SmB_6 nanowire photodetector reveals its application potential in mid-infrared photodetectors.

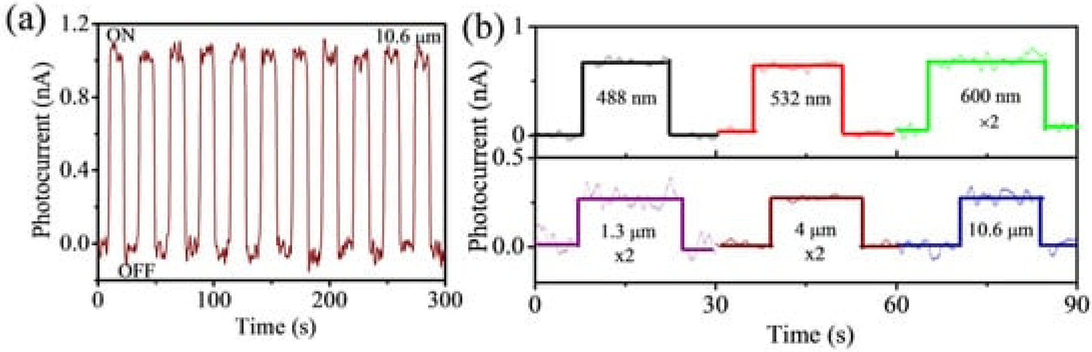

Figure 5. (**a**) Current–time measurement of SmB_6 nanowire photodetector under illuminating of 10.6 μm light source. (**b**) Current–time curves of SmB_6 nanowire photodetector under illuminating with different light wavelengths [46]. Copyright 2018, AIP Publishing.

2.3. Electrochemical Performances

RB_6 crystals show excellent metal-like conductivity (>10^3 S m^{-1}) and they are suitable for active electrochemical electrode materials for energy storage. Recently, Wang et al. [47] reported the application of CeB_6 nanowires as lithium-ion battery anode materials, and they obtained a capacity of ~225 mA h g^{-1} after 60 cycles (**Figure 6**a). The kinetic analysis shows that the Li^+ storage mechanism mainly comes from the surface capacitive behavior. Xue et al. [48] reported the LaB_6 nanowires on carbon fiber as electrode materials for supercapacitors (**Figure 6**b). The LaB_6 electrode materials showed a high areal capacitance of 17.34 mF cm^{-2} and revealed suitable cycling stability after 10,000 cycles. The successful application of RB_6 nanowires in batteries and capacitors demonstrates their potential in the field of electrochemical energy storage.

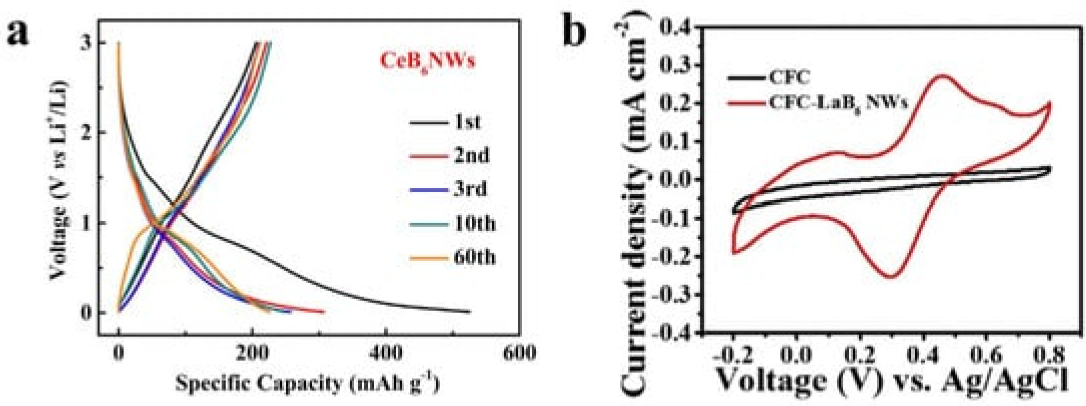

Figure 6. (**a**) The charge–discharge curves of CeB_6 nanowire electrodes for lithium-ion battery anodes [47]. (Copyright 2020, Elsevier Science B.V.) (**b**) CV curves of CFC and LaB_6-CFC electrode for supercapacitors [48]. (Copyright 2018, Elsevier Science B.V.)

References

1. Ji, X.H.; Zhang, Q.Y.; Xu, J.Q.; Zhao, Y.M. Rare-earth hexaborides nanostructures: Recent advances in materials, characterization and investigations of physical properties. Prog. Solid State Chem. 2011, 39, 51–69.

2. Carenco, S.; Portehault, D.; Boissiere, C.; Mezailles, N.; Sanchez, C. Nanoscaled metal borides and phosphides: Recent developments and perspectives. Chem. Rev. 2013, 113, 7981–8065.

3. Gan, H.; Zhang, T.; Guo, Z.; Lin, H.; Li, Z.; Chen, H.; Chen, J.; Liu, F. The growth methods and field emission studies of low-dimensional boron-based nanostructures. Appl. Sci. 2019, 9, 1019.

4. Kunii, S.; Kasuya, T.; Kadowaki, K.; Date, M.; Woods, S.B. Electron tunneling into superconducting YB6. Solid State Commun. 1984, 52, 659–661.

5. Zhang, H.; Tang, J.; Zhang, Q.; Zhao, G.; Yang, G.; Zhang, J.; Zhou, O.; Qin, L.-C. Field emission of electrons from single LaB6 nanowire. Adv. Mater. 2006, 18, 87–91.

6. Jang, H.; Friemel, G.; Ollivier, J.; Dukhnenko, A.V.; Shitsevalova, N.Y.; Filipov, V.B.; Keimer, B.; Inosov, D.S. Intense low-energy ferromagnetic fluctuations in the antiferromagnetic heavy-fermion metal CeB6. Nat. Mater. 2014, 13, 682–687.

7. Pohlit, M.; Rößler, S.; Ohno, Y.; Ohno, H.; Von Molnár, S.; Fisk, Z.; Müller, J.; Wirth, S. Evidence for ferromagnetic clusters in the colossal-magnetoresistance material EuB6. Phys. Rev. Lett. 2018, 120, 257201.

8. Li, L.; Sun, K.; Kurdak, C.; Allen, J.W. Emergent mystery in the Kondo insulator samarium hexaboride. Nat. Rev. Phys. 2020, 2, 463–479.

9. Zhang, H.; Zhang, Q.; Tang, J.; Qin, L.C. Single-crystalline LaB6 nanowires. J. Am. Chem. Soc. 2005, 127, 2862–2863.
10. Zhang, H.; Zhang, Q.; Tang, J.; Qin, L.C. Single-crystalline CeB6 nanowires. J. Am. Chem. Soc. 2005, 127, 8002–8003.
11. Zhang, H.; Zhang, Q.; Zhao, G.; Tang, J.; Zhou, O.; Qin, L.C. Single-crystalline GdB6 nanowire field emitters. J. Am. Chem. Soc. 2005, 127, 13120–13121.
12. Xu, J.; Zhao, Y.; Zou, C. Self-catalyst growth of LaB6 nanowires and nanotubes. Chem. Phys. Lett. 2006, 423, 138–142.
13. Zou, C.Y.; Zhao, Y.M.; Xu, J.Q. Synthesis of single-crystalline CeB6 nanowires. J. Cryst. Growth 2006, 291, 112–116.
14. Ding, Q.; Zhao, Y.; Xu, J.; Zou, C. Large-scale synthesis of neodymium hexaboride nanowires by self-catalyst. Solid State Commun. 2007, 141, 53–56.
15. Xu, J.; Chen, X.; Zhao, Y.; Zou, C.; Ding, Q.; Jian, J. Self-catalyst growth of EuB6 nanowires and nanotubes. J. Cryst. Growth 2007, 303, 466–471.
16. Xu, J.Q.; Zhao, Y.M.; Shi, Z.D.; Zou, C.Y.; Ding, Q.W. Single-crystalline SmB6 nanowires. J. Cryst. Growth 2008, 310, 3443–3447.
17. Brewer, J.R.; Deo, N.; Wang, Y.M.; Cheung, C.L. Lanthanum hexaboride nanoobelisks. Chem. Mater. 2007, 19, 6379–6381.
18. Wang, G.; Brewer, J.R.; Chan, J.Y.; Diercks, D.R.; Cheung, C.L. Morphological evolution of neodymium boride nanostructure growth by chemical vapor deposition. J. Phys. Chem. C 2009, 113, 10446–10451.
19. Brewer, J.R.; Jacobberger, R.M.; Diercks, D.R.; Cheung, C.L. Rare earth hexaboride nanowires: General synthetic design and analysis using atom probe tomography. Chem. Mater. 2011, 23, 2606–2610.
20. Chi, M.; Zhao, Y.; Fan, Q.; Han, W. The synthesis of PrB6 nanowires and nanotubes by the self-catalyzed method. Ceram. Int. 2014, 40, 8921–8924.
21. Zhang, H.; Tang, J.; Yuan, J.; Ma, J.; Shinya, N.; Nakajima, K.; Murakami, H.; Ohkubo, T.; Qin, L.-C. Nanostructured LaB6 field emitter with lowest apical work function. Nano Lett. 2010, 10, 3539–3544.
22. Xu, J.; Chen, X.; Zhao, Y.; Zou, C.; Ding, Q. Single-crystalline PrB6 nanowires and their field-emission properties. Nanotechnology 2007, 18, 115621.
23. Xu, J.Q.; Zhao, Y.M.; Zhang, Q.Y. Enhanced electron field emission from single-crystalline LaB6 nanowires with ambient temperature. J. Appl. Phys. 2008, 104, 124306.

24. Xu, J.Q.; Zhao, Y.M.; Ji, X.H.; Zhang, Q.; Lau, S.P. Growth of single-crystalline SmB6 nanowires and their temperature-dependent electron field emission. J. Phys. D Appl. Phys. 2009, 42, 135403.
25. Zhang, Q.Y.; Xu, J.Q.; Zhao, Y.M.; Ji, X.H.; Lau, S.P. Fabrication of large-scale single-crystalline PrB6 nanorods and their temperature-dependent electron field emission. Adv. Funct. Mater. 2009, 19, 742–747.
26. Xu, J.; Hou, G.; Li, H.; Zhai, T.; Dong, B.; Yan, H.; Wang, Y.; Yu, B.; Bando, Y.; Golberg, D. Fabrication of vertically aligned single-crystalline lanthanum hexaboride nanowire arrays and investigation of their field emission. NPG Asia Mater. 2013, 5, e53.
27. Xu, J.; Hou, G.; Mori, T.; Li, H.; Wang, Y.; Chang, Y.; Luo, Y.; Yu, B.; Ma, Y.; Zhai, T. Excellent field-emission performances of neodymium hexaboride (NdB6) nanoneedles with ultra-low work functions. Adv. Funct. Mater. 2013, 23, 5038–5048.
28. Li, Q.; Zhang, H.; Chen, J.; Zhao, Y.; Han, W.; Fan, Q.; Liang, Z.; Liu, X.; Kuang, Q. Single-crystalline LaxNd1−xB6 nanowires: Synthesis, characterization and field emission performance. J. Mater. Chem. C 2015, 3, 7476–7482.
29. Zhang, H.; Tang, J.; Zhang, L.; An, B.; Qin, L.C. Atomic force microscopy measurement of the Young's modulus and hardness of single LaB6 nanowires. Appl. Phys. Lett. 2008, 92, 173121.
30. Han, W.; Zhang, H.; Chen, J.; Zhao, Y.; Fan, Q.; Li, Q.; Liu, X.; Lin, X. Single-crystalline LaxPr1-xB6 nanoawls: Synthesis, characterization and growth mechanism. Ceram. Int. 2016, 42, 6236–6243.
31. Gan, H.; Ye, B.; Zhang, T.; Xu, N.; He, H.; Deng, S.; Liu, F. A controllable solid-source CVD route to prepare topological Kondo insulator SmB6 nanobelt and nanowire arrays with high activation energy. Cryst. Growth Des. 2019, 19, 845–853.
32. Han, W.; Qiu, Y.; Zhao, Y.; Zhang, H.; Chen, J.; Sun, S.; Lan, L.; Fan, Q.; Li, Q. Low-temperature synthesis and electronic transport of topological insulator SmB6 nanowires. CrystEngComm 2016, 18, 7934–7939.
33. Kong, L.J.; Zhou, Y.; Liu, S.; Lin, Z.; Zhang, L.; Lin, F.; Tang, D.S.; Wu, H.C.; Liu, J.F.; Lu, H.Z.; et al. Spin-polarized surface state transport in a topological Kondo insulator SmB6 nanowire. Phys. Rev. B 2017, 95, 235410.
34. Zhou, L.; Ye, B.C.; Gan, H.B.; Tang, J.Y.; Chen, P.B.; Du, Z.Z.; Tian, Y.; Deng, S.Z.; Guo, G.P.; Lu, H.Z.; et al. Surface-induced positive planar Hall effect in topological Kondo insulator SmB6 microribbons. Phys. Rev. B 2019, 99, 155424.
35. He, X.S.; Gan, H.B.; Du, Z.Z.; Ye, B.C.; Zhou, L.; Tian, Y.; Deng, S.Z.; Guo, G.P.; Lu, H.Z.; Liu, F.; et al. Magnetoresistance anomaly in topological Kondo insulator SmB6 nanowires with strong surface magnetism. Adv. Sci. 2018, 5, 1700753.

36. Kong, L.J.; Zhou, Y.; Song, H.D.; Yu, D.P.; Liao, Z.M. Magnetoresistance hysteresis in topological Kondo insulator SmB6 nanowire. Chin. Phys. B 2019, 28, 107501.
37. Gan, H.; Ye, B.; Zhou, L.; Zhang, T.; Tian, Y.; Deng, S.; He, H.; Liu, F. Controllable synthesis of Gd-doped SmB6 nanobelt arrays for modulating their surface transport behaviors. Mater. Today Nano 2020, 12, 100097.
38. Kang, C.J.; Denlinger, J.D.; Allen, J.W.; Min, C.H.; Reinert, F.; Kang, B.Y. Electronic structure of YbB6: Is it a topological insulator or not? Phys. Rev. Lett. 2016, 116, 116401.
39. Zhou, Y.; Kim, D.J.; Rosa, P.F.S.; Wu, Q.; Guo, J.; Zhang, S.; Wang, Z.; Kang, D.; Zhang, C.; Yi, W.; et al. Pressure-induced quantum phase transitions in a YbB6 single crystal. Phys. Rev. B 2015, 92, 241118.
40. Munarriz, J.; Robinson, P.J.; Alexandrova, A.N. Towards a single chemical model for understanding lanthanide hexaborides. Angew. Chem. 2020, 132, 22873–22878.
41. Han, W.; Wang, Z.; Li, Q.; Liu, H.; Fan, Q.; Dong, Y.; Kuang, Q.; Zhao, Y. Autoclave growth, magnetic, and optical properties of GdB6 nanowires. J. Solid State Chem. 2017, 256, 53–59.
42. Wang, Z.; Han, W.; Zhang, J.; Fan, Q.H.; Zhao, Y.M. Superconducting YB6 nanowires. Ceram. Int. 2021, 47, 23788–23793.
43. Zhang, H.; Tang, J.; Yuan, J.S.; Yamauchi, Y.; Suzuki, T.T.; Shinya, N.; Nakajima, K.; Qin, L.C. An ultrabright and monochromatic electron point source made of a LaB6 nanowire. Nat. Nanotech. 2016, 11, 273.
44. Zhang, H.; Jimbo, Y.; Niwata, A.; Ikeda, A.; Yasuhara, A.; Ovidiu, C.; Kimoto, K.; Kasaya, T.; Miyazaki, H.T.; Tsujii, N.; et al. High-endurance micro-engineered LaB6 nanowire electron source for high-resolution electron microscopy. Nat. Nanotechnol. 2021, 1–6.
45. Tang, S.; Tang, J.; Wu, Y.M.; Chen, Y.-H.; Uzuhashi, J.; Ohkubo, T.; Qin, L.-C. Stable field-emission from a CeB6 nanoneedle point electron source. Nanoscale 2021, 13, 17156–17161.
46. Zhou, Y.; Lai, J.W.; Kong, L.J.; Ma, J.C.; Lin, Z.L.; Lin, F.; Zhu, R.; Xu, J.; Huang, S.M.; Tang, D.S.; et al. Single crystalline SmB6 nanowires for self-powered, broadband photodetectors covering mid-infrared. Appl. Phys. Lett. 2018, 112, 162106.
47. Wang, Z.; Han, W.; Kuang, Q.; Fan, Q.; Zhao, Y. Low-temperature synthesis of CeB6 nanowires and nanoparticles as feasible lithium-ion anode materials. Adv. Powder Tech. 2020, 31, 595–603.
48. Xue, Q.; Tian, Y.; Deng, S.Z.; Huang, Y.; Zhu, M.S.; Pei, Z.X.; Li, H.F.; Liu, F.; Zhi, C.Y. LaB6 nanowires for supercapacitors. Mater. Today Energy 2018, 10, 28–33.